Journal of Hazardous Materials 173 (2010) 614–621

Contents lists available at ScienceDirect

Journal of Hazardous Materials

journal homepage: www.elsevier.com/locate/jhazmat

Research article

Removal of hexavalent chromium [Cr(VI)] from aqueous solutions by the diatomite-supported/unsupported magnetite nanoparticles

Peng Yuan[a,*], Dong Liu[a,b], Mingde Fan[a,b], Dan Yang[a,b], Runliang Zhu[c], Fei Ge[c], JianXi Zhu[a], Hongping He[a]

[a] Guangzhou Institute of Geochemistry, Chinese Academy of Sciences, Guangzhou 510640, China
[b] Graduate School of Chinese Academy of Sciences, Beijing 100039, China
[c] College of Chemical Engineering, Xiangtan University, Xiangtan 411105, China

ARTICLE INFO

Article history:
Received 21 March 2009
Received in revised form 26 August 2009
Accepted 26 August 2009
Available online 1 September 2009

Keywords:
Magnetite
Diatomite
Chromium
Adsorption
Transmission electron microscopy

ABSTRACT

Diatomite-supported/unsupported magnetite nanoparticles were prepared by co-precipitation and hydrosol methods, and characterized by X-ray diffraction, nitrogen adsorption, elemental analysis, differential scanning calorimetry, transmission electron microscopy and X-ray photoelectron spectroscopy. The average sizes of the unsupported and supported magnetite nanoparticles are around 25 and 15 nm, respectively. The supported magnetite nanoparticles exist on the surface or inside the pores of diatom shells, with better dispersing and less coaggregation than the unsupported ones. The uptake of hexavalent chromium [Cr(VI)] on the synthesized magnetite nanoparticles was mainly governed by a physico-chemical process, which included an electrostatic attraction followed by a redox process in which Cr(VI) was reduced into trivalent chromium [Cr(III)]. The adsorption of Cr(VI) was highly pH-dependent and the kinetics of the adsorption followed a pseudo-second-order model. The adsorption data of diatomite-supported/unsupported magnetite fit well with the Langmuir isotherm equation. The supported magnetite showed a better adsorption capacity per unit mass of magnetite than unsupported magnetite, and was more thermally stable than their unsupported counterparts. These results indicate that the diatomite-supported/unsupported magnetite nanoparticles are readily prepared, enabling promising applications for the removal of Cr(VI) from aqueous solution.

1. Introduction

Magnetite (Fe_3O_4) nanoparticles have attracted increasing research interest in the fields of catalysis and environmental remediation in recent years [1,2]. This is because magnetite nanoparticles possess not only strong adsorption/reduction activities, but also the property of being easily separated and collected by an external magnetic field [3,4]. The good adsorption activities of magnetite nanoparticles for many heavy metal ions have been reported in literatures [5–7].

As well known, the coaggregation problem often constitutes a challenge that nanoparticles have to be confronted, since the coaggregation decreases the effective surface area of nanoparticles and thus reduces their reaction activities. Several methods have been developed to overcome the coaggregation problem. Organized assemblies such as surfactant matrix [8,9] and silica microspheres [10] were applied as dispersants to control the coaggregation of the iron oxide nanoparticles. Supporting of magnetite nanoparticles on polymer [11,12], porous silica [13], clays [14] and zeolite [15] during the preparation process were also found to be effective to prevent coaggregation. The resulting heterogeneous systems showed better performance in recycling use with lower cost than their homogeneous counterparts. In this sense, it would be very interesting to synthesize supported magnetite nanoparticles and to explore the effect of the support on the related characteristics and activities of the nanoparticles.

Diatomite is a fossil assemblage of diatom shells. Composed of biogenetic amorphous silica, diatom shell is characteristic of macro/mesoporous structure and excellent thermal and mechanical stabilities [16–19]. As a low-cost and readily available mineral with highly developed porous structure, diatomite may be particularly suitable to be used as a support for the synthesis of magnetite nanoparticles. However, so far, few attempts to synthesize diatomite-supported magnetite nanoparticles could be found in literatures.

In the present study, we prepared diatomite-supported magnetite nanoparticles and used the nanocompostie as adsorbent for the removal of hexavalent chromium [Cr(VI)]. Cr(VI) is a highly toxic agent that is carcinogenic, mutagenic and teratogenic to living organisms [20]. Mainly existing in the forms of anions of

* Corresponding author. Tel.: +86 20 85290341; fax: +86 20 85290341.
E-mail address: yuanpeng@gig.ac.cn (P. Yuan).

0304-3894/$ – see front matter © 2009 Elsevier B.V. All rights reserved.
doi:10.1016/j.jhazmat.2009.08.129

chromate and dichromate in aqueous systems, Cr(VI) is usually released from various industrial operations such as metallurgy and leather tanning [21]. Cr(VI)-containing wastewater from these processes is typically disposed by means of domestic sewage systems with little treatment in some undeveloped areas. A variety of methods have been developed for the removal of Cr(VI) from wastewater, such as adsorption, ion exchange, chemical precipitation, electro-deposition and reverse osmosis [6,22–24]. Among these methods chemical reduction followed by precipitation or adsorption is the most widely used technique [25]. With this method Cr(VI) is converted into trivalent chromium [Cr(III)] with much lower toxicity and limited hydroxide solubility. The reduction agents used for the converting process include iron sulfide [26], ferrous iron [27], ferrite [28], various types of metallic iron and zero-valent iron [29–34], green rust [35], siderite [36] and magnetite [37,38]. However, less research attention was paid to using supported nano-scaled magnetite as a reduction agent or an adsorbent for the treatment of Cr(VI).

Consequently, the objective of this study is to assess the feasibility of applying diatomite-supported magnetite nanoparticles for the removal of Cr(VI) from aqueous solutions. For this purpose, the prepared supported/unsupported magnetite nanoparticles were tested in a series adsorption experiments, and several chemical, spectroscopic and microscopic characterization methods were used to investigate how the characteristics of materials and the condition-specific parameters affect the reaction mechanism.

2. Materials and methods

2.1. Materials and preparation methods

Raw diatomite from Guangdong, China, was purified by the method described in our previous report [39]. The chemical composition (wt%) of the purified diatomite (Dt) is: SiO_2, 90.1; Fe_2O_3, 0.3; CaO, 0.5; MgO, 0.2; TiO_2, 0.4; loss, 7.9. The transmission electron microscope (TEM) characterization shows that most diatoms in the sample belong to the genera *Synedra ulna* (Nitz.) Ehr., and have width of 3–15 μm and length of 40–120 μm. Analytical grade reagents such as $FeCl_3{\cdot}6H_2O$ (99%), $FeCl_2{\cdot}4H_2O$ (99%) and NH_4OH were used for the synthesis of magnetite. $K_2Cr_2O_7$ (99%) was used for the preparation of Cr(VI) solution.

The magnetite nanoparticles (Mag) were prepared by the following steps: the powder of $FeCl_3{\cdot}6H_2O$ and $FeCl_2{\cdot}4H_2O$, with a molar ratio of Fe(II)/Fe(III) = 1/2, were dissolved in distilled water that had just been deoxygenated by bubbling N_2 gas for 30 min. The amount of the added iron salt was about 3 g in 200 mL water. The solution was kept under N_2 protection and vigorously stirring for 5 min in a water bath at 60 °C. After that NH_4OH solution (1.5 M) was slowly added into the Fe(II)/Fe(III) solution. The addition was stopped when the pH value of the mixture reached 8.0. Then the mixture was aged for 30 min at 60 °C. The precipitate was isolated by using an external magnetic field and the supernatant was decanted. The obtained solid part was quickly washed four times with deionizated and deoxygenated water and dried at 40 °C under vacuum.

Two methods were applied to prepare diatomite-supported magnetite nanoparticles. One was the co-precipitation method in which the diatomite powder was simply added into the mixed solution of ferric chloride and ferrous chloride before the addition of ammonia solution, with a ratio of 10 mmol Fe per gram of diatomite. And the rest preparation process followed the same steps as the preparation of Mag. The resultant sample was denoted as MagDt-P.

For the other preparation method, the hydrosol of magnetite was firstly synthesized and then loaded on diatomite. Synthesis of the magnetite hydrosol followed a preparation route proposed by Kang et al. [40]. The resultant magnetite hydrosol, which was a clear and transparent cationic colloid with pH value about 4.0, was left to stand for a few hours to settle out any residual solids. The dark-colored supernatant was separated for further preparation. In a run for the preparation of diatomite-supported magnetite, a 5% (wt%) diatomite suspension was added into the magnetite hydrosol with equivalent volume. The mixture was stirred for 30 min, and then centrifuged at 4000 rpm for 5 min. It was observed that the supernatant liquid of the mixture became colorless, which indicated that the positively charged magnetite nanoparticles were completely adsorbed by the negatively charged diatomite particles by electrostatic attraction. The colorless supernatant was discarded, and the solid part was further mixed with magnetite hydrosol and the mixture was stirred and centrifuged again. The above treatment cycle was ended until the supernatant did not anymore become colorless, which was an indication of the saturated adsorption of magnetite hydrosol onto the diatomite. The resultant solid was separated and dried at 40 °C under vacuum. The diatomite-supported magnetite prepared by this method was referred to as MagDt-H.

All prepared samples were kept on a vacuum desiccator before being used for adsorption experiments. To test the stability of the supported/unsupported magnetite nanoparticles over a long-term, a portion of each sample was kept under ambient condition in a covered container for 2 years. The obtained samples were differentiated by the suffix -T (e.g. Mag-T). Moreover, a commercial magnetite (MicroMag), which has an average of particle size of ca. 20 μm, was used in the adsorption tests for comparison purpose.

2.2. Adsorption experiments

In a typical run, 0.5 g adsorbent was added into 100 mL of Cr(VI) solution with scheduled concentration in a 125 mL high density poly(ethylene) (HDPE) bottle. No buffer was added in these experiments. The Cr(VI) solution was prepared by dissolving $K_2Cr_2O_7$ in distilled water. The pH value was adjusted by 0.1 M HNO_3 and 0.1 M NaOH solution. For the kinetics tests, the mixture in the HDPE bottle was strongly shaken at a rate of 160 rpm in an oscillator to ensure a complete mixing. The contact time was in the range from 2 to 120 min. At timed intervals, samples were taken by HDPE 3 mL syringe and filtered through a 0.2 μm cellulose acetate syringe filters. The Cr(VI) content in the filtered solution was measured by using a Shimadzu UV-260 Spectrophotometer according to the determination procedure described in literature [41]. The experiments for obtaining adsorption isotherms followed a very similar procedure except for the equilibrium time was fixed as 120 min. All adsorption experiments were conducted at room temperature (25 ± 2 °C) unless noted, and all of the adsorption results were corrected by blank tests in which no adsorbent was added into the Cr(VI) solution. The amount of Cr(VI) adsorbed per unit mass of the adsorbent, q (mg/g), was computed by using the expression: $q = (C_0 - C_t)/m$, where C_0 and C_t (mg/L) are the concentration of Cr(VI) in the reaction solution before and after treatment, respectively, and m (g) is the amount of adsorbents in 1 L of Cr(VI) solution. The removal efficiency of Cr(VI), E (%), was calculated using the equation: $E = [(C_0 - C_t)/C_0] \times 100$.

2.3. Characterization methods

X-ray diffraction (XRD) patterns were recorded at a scanning rate of 4°/min on a Rigaku D/Max 2200 VPC diffractometer, equipped with a graphite-monochromatized Cu Kα radiation course (λ = 0.154 nm) under target voltage 40 kV and current 30 mA. The chemical compositions of the samples were determined using a PE-3100 atomic absorption spectrometer (AAS). N_2 adsorption–desorption isotherms were measured on a Micromeritics ASAP 2020 system at liquid nitrogen temperature. The samples

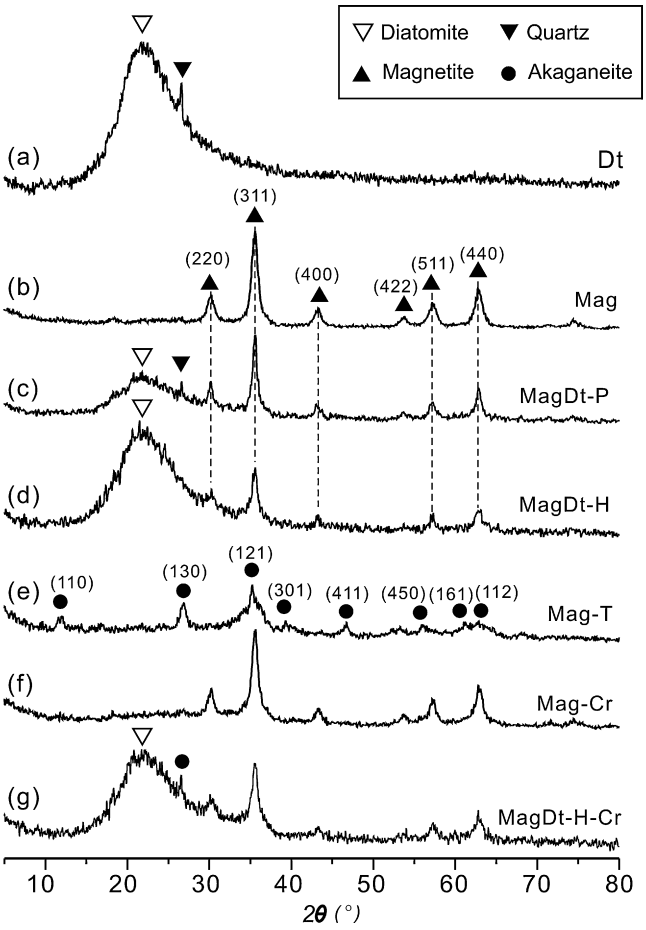

Fig. 1. XRD patterns of the diatomite and the unsupported/diatomite-supported magnetite samples.

were outgassed at 350 °C for 8 h before measurement. The specific surface area, S_{BET}, was calculated by using the multiple-point Brunauer–Emmett–Teller (BET) method [42] and the total pore volume, V_{pore}, was evaluated from nitrogen uptake at a relative pressure of ca. 0.97. The pore size distribution was computed by using the Barrett–Joyner–Halenda (BJH) method [43]. TEM images were obtained on a Philips CM120 electron microscope operating at an acceleration voltage of 120 kV. Differential scanning calorimetry (DSC) characterization was performed on a Netzsch STA 409 PC instrument. Approximately 10 mg of finely ground sample was heated in a corundum crucible with a heating rate of 5 °C/min under air atmosphere. X-ray photoelectron spectroscopy (XPS) analyse was performed on a Kratos AXIS Ultra with a monochromatic Al X-ray source at 150 W.

3. Results and discussion

3.1. Characterization of the diatomite-supported/unsupported magnetite nanoparticles

The XRD pattern of Dt (Fig. 1a) is in good agreement with that of the referenced amorphous silica, characteristic of a broad peak centered at ca. 21.8°. The diffraction pattern of Mag (Fig. 1b) exhibits distinct plane distances of 0.296, 0.253, 0.209, 0.161, and 0.148 nm, which are well consistent with the referenced data of 0.297, 0.253, 0.209, 0.162, and 0.149 nm for (2 2 0), (3 1 1), (4 0 0), (5 1 1) and (4 4 0) plane distances, respectively [44]. Fig. 1c and d presents the XRD patterns of diatomite-supported magnetite prepared via co-precipitation (MagDt-P) and hydrosol method

Table 1
The total Fe_3O_4 content and the porous structural data of the prepared samples.

Samples	Mag	MicroMag	Dt	MagDt-P	MagDt-H
Fe_3O_4 (%)	92.8	94.0	–	31.6	17.8
S_{BET} (m^2/g)	86.6	26.1	10.9	50.2	24.1
V_{pore} (cm^3/g)	0.32	0.11	0.04	0.13	0.08

(MagDt-H), respectively. In both curves, the broad peak resulting from the diatomite support and the reflections corresponding to magnetite are presented simultaneously. And the content of magnetite in MagDt-P is higher than that of MagDt-H, based on a semi-quantitatively calculation by use of deconvolution of XRD peaks. This is in accordance with the chemical analysis result (Table 1) that the content of Fe_3O_4 in MagDt-P (31.6 wt%) is higher than that in MagDt-H (17.8 wt%). Sample Mag-T, obtained by placing Mag under ambient condition for two years, shows a XRD pattern attributed to akaganeite (β-FeOOH) (Fig. 1e). The akaganeite phase should result from the long-term reaction between the ambient water and the magnetite. However, the XRD patterns of MagDt-P-T and MagDt-H-T (not shown) just resemble those of MagDt-P and MagDt-H, respectively. This indicates the magnetite was prevented from transforming into akaganeite, which was probably due to that the surface hydroxyl groups of diatomite adsorbed the ambient water and effectively reduced the contact between water molecules and magnetite. This result suggests that diatomite support has good effect on enhancing the stability of the nano-scaled magnetite and is very useful for its storage and transportation.

As displayed in the DSC curve of Mag (Fig. 2a), an exothermic signal at ca. 187 °C is resolved, which corresponds to the beginning temperature of the transformation from magnetite to maghemite (γ-Fe_2O_3) [45]. This transformation appears a multi-step process, which is composed of gradual transformation of the magnetite nanoparticles with different sizes and ends at ca. 349 °C (Fig. 2a). The exothermic signal at 516 °C is attributed to the transformation from maghemite to hematite (α-Fe_2O_3). These two thermal events are consistent with the previously reported phase-transformation temperature range of magnetite [44–46]. As compared to Mag, MagDt-P exhibits weaker signals of the transformation from magnetite to maghemite, which begins at about 250 °C and finishes at ca. 432 °C (Fig. 2b). Meanwhile, exothermic signal of the phase transformation from maghemite to hematite for MagDt-P centers at about 650 °C. The higher phase-transformation temperature of

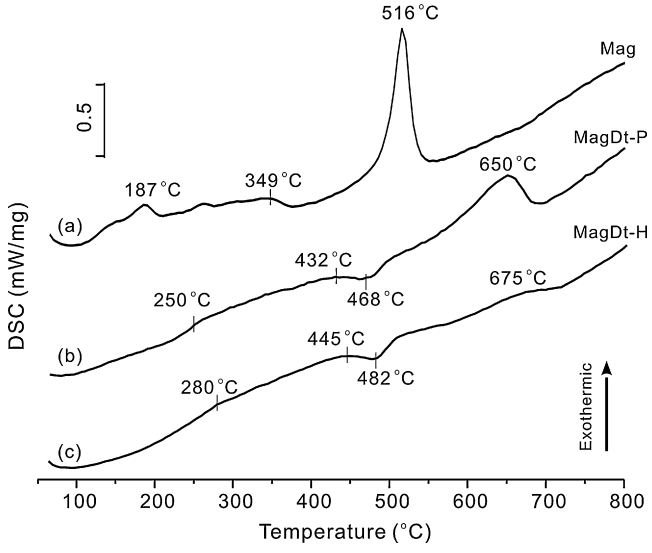

Fig. 2. DSC curves of the unsupported/diatomite-supported magnetite samples.

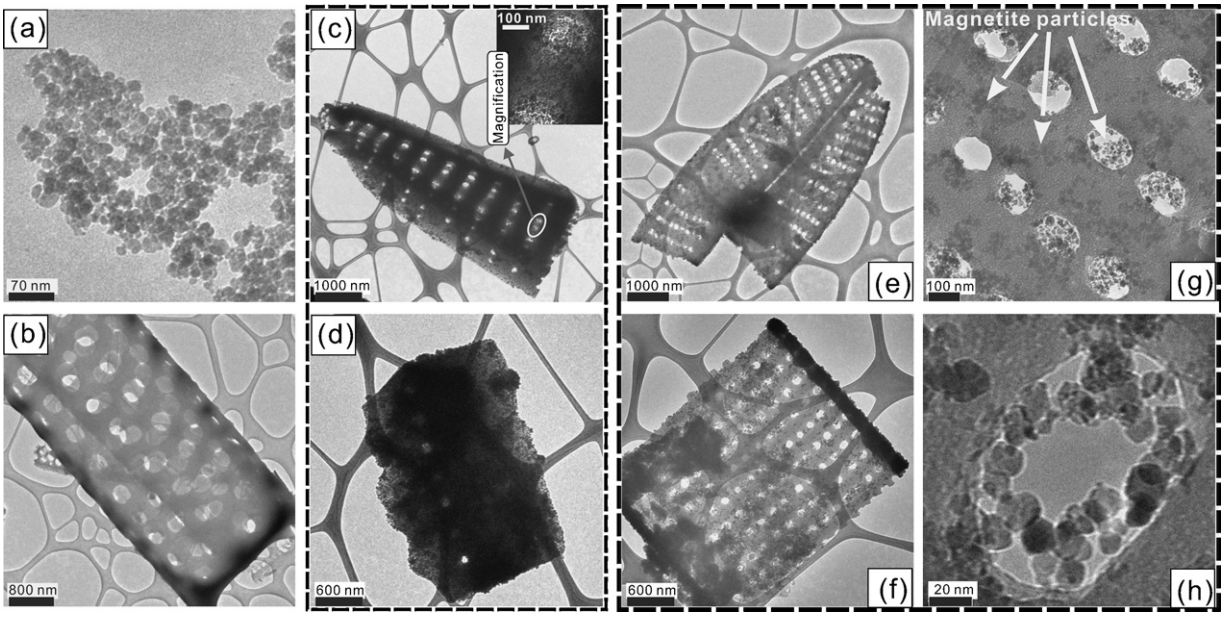

Fig. 3. TEM images of (a) Mag; (b) Dt; (c and d) two diatom shells in MagDt-P; (e and f) two diatom shells in MagDt-H; (g and h) sample MagDt-H with high resolution.

MagDt-P relative to that of Mag suggests the diatomite support increased the thermal stabilities of the magnetite nanoparticles. This is due to the nanoparticles were effectively separated by the diatom shells, therefore many of them were prevented from aggregating and further transforming. A similar phenomenon was also found in the system of clay-supported iron/titanium oxides [47,48]. The DSC curve of MagDt-H is analogous to that of MagDt-P (Fig. 2c), but the phase-transformation signals of iron oxides for MagDt-H are weaker than those for MagDt-P. This is because the content of magnetite in MagDt-H is lower than that in MagDt-P.

The TEM image of Mag (Fig. 3a) shows that the synthesized magnetite nanoparticles have an average size around 25 nm and dramatically coaggregate together. The diatom shells in diatomite exhibit clear porous structure and clean surface (Fig. 3b). MagDt-P shows a high extent of loading of magnetite, as indicated by that the magnetite nanoparticles coaggregated with each other through the surface or even filled in the pores of the diatom shells (Fig. 3c and d), which significantly reduced the visibility of the porous structure of diatomite. In MagDt-P unsupported magnetite nanoparticles were also found, and they exhibit similar coaggregation characteristics and sizes to those in Mag (TEM images are not shown). In contrast with that, in MagDt-H almost no separate coaggregates of unloaded magnetite nanoparticles were observed and the porous structure of diatomite remained clearly visible (Fig. 3e and f). From the TEM images of MagDt-H with higher resolution, it can be seen that the magnetite nanoparticles were better dispersed at the surface (Fig. 3g) or within the pores (Fig. 3h) than those in MagDt-P. Meanwhile, the average size of the nanoparticles in MagDt-H is about 15 nm, much smaller than that in Mag. These comparisons suggest that the diatomite-supported magnetite prepared via hydrosol route is better in enhancing the dispersion of magnetite nanoparticles than that via co-precipitate route, although the latter one shows a larger loading quantity of magnetite.

As shown in Fig. 4, the nitrogen adsorption–desorption isotherm of Mag belong to the type II with H3 hysteresis loop, according to IUPAC-classification [42]. The hysteresis loop of this isotherm is associated with the filling and emptying of the mesopores by capillary condensation. These mesopores should be the spaces between magnetite nanoparticles since magnetite is actually nonporous as already known. Dt exhibits an isotherm of type II with a very minor hysteresis loop, which is in agreement with the previous report that diatomite is mainly macroporous with small amount of mesopores [49]. Represented in the inset of Fig. 4 is the pore size distribution (PSD) curves calculated from the BJH method. The primary peak at ca. 15 nm in the curve of Mag corresponds to the main population of pores, and can be readily identified as the interspaces between magnetite particles. In contrast, Dt shows a broader pore distribution in which pores with different sizes coexist. As compared to Mag, MagDt-P exhibits an isotherm with less developed hysteresis loop, implying the volume of the mesopores between magnetite nanoparticles was reduced. The primary peak in the PSD curve of MagDt-P located at a lower value (ca. 8 nm), reflecting the mesopores resulting from interspaces of magnetite nanoparticles became smaller. MagDt-H exhibits an isotherm with minor hysteresis loop and a PSD curve without dramatic peak. This feature is very close to that of Dt, indicating the magnetite nanoparticles were well dispersed on the diatom shells and the interspaces between magnetite particles were significantly diminished. These above proposals are evidenced by the data of the specific surface area and the porous volume (Table 1), which follow an order of

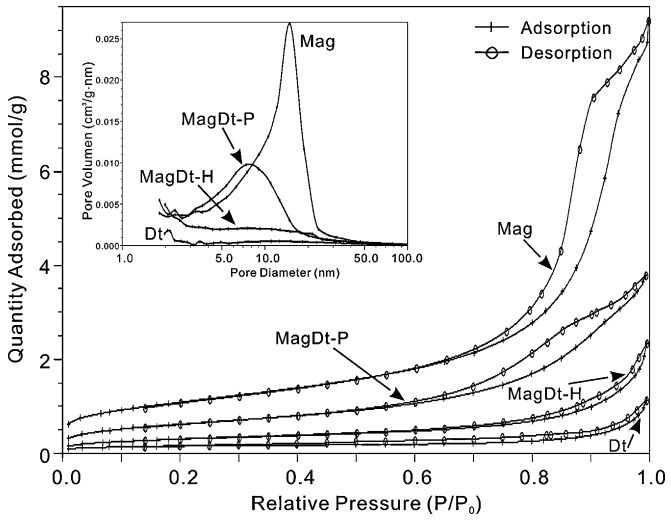

Fig. 4. Nitrogen adsorption–desorption isotherms and PSD curves (the insert) of diatomite and the unsupported/diatomite-supported magnetite samples.

Mag > MagDt-P > MagDt-H > Dt. This result is also in good agreement with the XRD results (Fig. 1), the chemical analysis (Table 1) and the TEM observation (Fig. 3).

3.2. Kinetics and isotherms of the Cr(VI) adsorption on diatomite-supported/unsupported magnetite nanoparticles

Due to its better dispersion performance of the magnetite nanoparticles, MagDt-H was chosen for the adsorption tests in this study. It is noteworthy that possibly the dispersion performance of MagDT-P could be improved with revisions of the preparation methodology; however, testing on this front will be done as part of another investigation. Before the batch experiments, effects of pH values on the adsorption of Cr(VI) were investigated to determine the optimum pH value applied in the adsorption tests. Because the pH dependence of magnetite is likely to control the pH dependence of both supported and unsupported magnetite systems, the supported magnetite (MagDT-H) was not directly tested. Instead we use the optimum pH values found for the magnetite samples. We additionally tested the Dt sample; however, it adsorbs so little Cr that it was not considered when picking the pH for the batch experiments, described in detail below. Mag, MicroMag and Dt were used as adsorbents for this investigation. Before addition of the adsorbents, the initial pH values were adjusted to the range of 2.0–9.0. The initial Cr(VI) concentration was set as 50 mg/L and the agitation time was 120 min. The maximum removal efficiency (ca. 99.8%) of Mag was found at pH 2.0–2.5, and at higher pH values the amount of Cr(VI) uptake decreased gradually (Fig. 5a). This result is in good agreement with the previous report [6], and can be explained as follows: different species of Cr(VI) ($Cr_2O_7^{2-}$, $HCrO_4^-$, $Cr_3O_{10}^{2-}$, $Cr_4O_{13}^{2-}$) coexist at acidic pH condition. At pH 2–3 the predominant Cr(VI) species is $HCrO_4^-$, which is favorable adsorbed since it has a low adsorption free energy [50]. The dramatic decrease of the Cr(VI) uptake with the increase of pH values was mainly due to that higher pH values made the surface of magnetite more negatively charged, which greatly enhanced the electrostatic repulsion between magnetite and Cr(VI) anions, leading to a release of the adsorbed Cr(VI) species from the magnetite surface. The uptake of Cr(VI) on MicroMag shows a similar pH-dependency to that of Mag, but with much lower removal efficiency (the maximum is about 40% of Mag's) at the same pH values (Fig. 5a). The maximum removal efficiency (ca. 10%) by Dt occurs at pH 1.0 (Fig. 5a). Such low adsorption of Cr(VI) on Dt should be attributed to the low pH_{ZPC} (~2.0) of diatomite [19], since the adsorption of the anionic Cr(VI) species are only favored when pH value is below 2.0. Considering the removal efficiency of Dt remained at a low level throughout the whole pH range, all subsequent adsorption experiments herein were conducted at pH 2.5, the optimum pH for adsorption of Cr(VI) on Mag and MicroMag.

Fig. 5b displays the removal of Cr(VI) by Mag, MicroMag and MagDt-H as a function of time. The plots of the amount of Cr(VI) adsorbed on the three adsorbents, normalized to the actual Fe_3O_4 content (Table 1), were presented as Fig. 5c. The initial Cr(VI) concentration was set as 50 mg/L. The Cr(VI) uptake was quite fast toward the beginning, followed by a much slower subsequent removal and at last leading to a steady state. About 90% of the Cr(VI) was removed by Mag during the first 2 min of the reaction, while only a small part of the additional removal occurred during the rest contact time. MagDt-H shows a similar rapid adsorption for Cr(VI), in which the uptake of more than 90% of the totally adsorbed Cr(VI) species was finished in the first 5 min (Fig. 5b). The rapid adsorption of Cr(VI) by Mag and MagDt-H may be attributed to the external surface adsorption. This suggests most of the adsorption sites of the nanoparticles existed in the exterior of the adsorbent and were easily accessible by the Cr(VI) species, resulting in a rapid approach to steady state. For both adsorbents, the steady state was

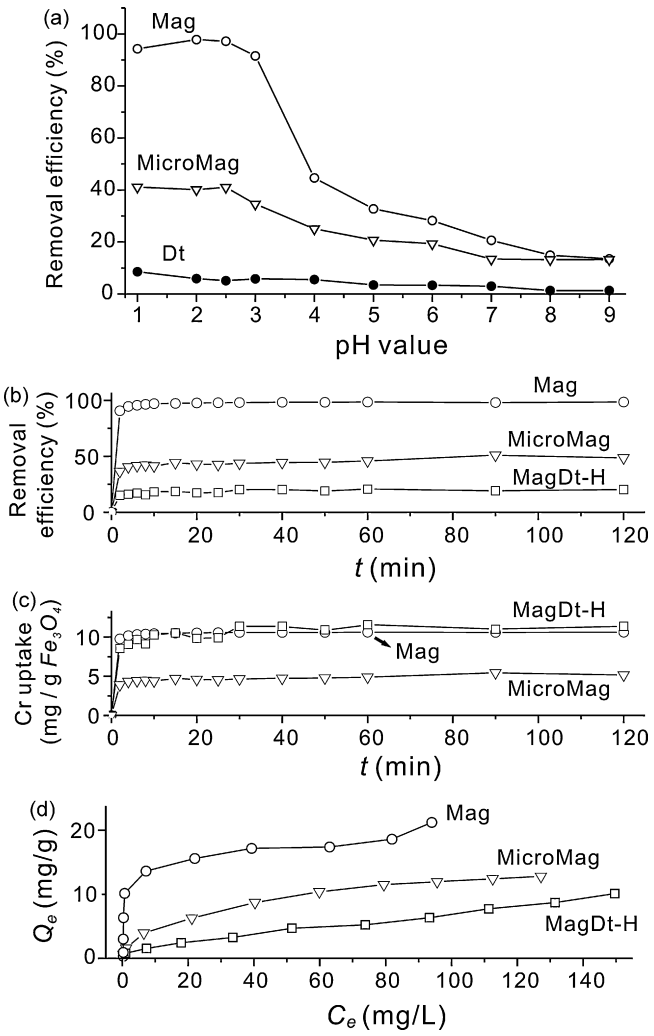

Fig. 5. (a) Effect of initial solution pH values on the removal of Cr(VI) on Mag, MicroMag and Dt; (b) effect of agitation time on the Cr(VI) removal efficiency of Mag, MicroMag and MagDt-H; (c) effect of agitation time on the normalized Cr uptake to actual Fe_3O_4 content; and (d) the Cr(VI) adsorption isotherms of Mag, MicroMag and MagDt-H.

achieved in 1 h. In comparison, this time length of Cr(VI) adsorption onto the diatomite-supported/unsupported magnetite nanoparticles is close to that of maghemite nanoparticle (about 20–60 min) [51], and is much higher than those of MicroMag (about 90 min, Fig. 5b), peat (~6 h) [52], volcanic ash (~6 h) [53], and activated carbon (about 10–70 h) [54,55].

The kinetics curve of the adsorption process was simulated using the pseudo-second-order model [56,57] with the rate expression given by

$$\frac{dq_t}{dt} = k_p(q_e - q_t)^2 \quad (1)$$

where k_p is the second order rate constant (g/(mg min)), q_t and q_e are the amount of Cr(VI) adsorbed per unit mass (mg/g) at any time (t) and at equilibrium, respectively. As shown in Table 2 for the simulation results, the sorption of Cr(VI) onto Mag, MicroMag and MagDt-H fits Eq. (1) quite well. This indicates that this sorption system is a pseudo-second-order reaction, implying the rate-limiting step may be chemical sorption involving valency forces through sharing or exchange of electrons between sorbent and sorbate [56].

To compare the Cr(VI) removal efficiency of unsupported/diatom-supported magnetite, the amount of Cr(VI) adsorbed per unit mass (g) of actual magnetite content, q_{e-s}, was

Table 2
Kinetics constants and Langmuir equation parameters for Cr(VI) adsorption on various adsorbents.

Adsorbents	Kinetics constants					Langmuir equation parameters			
	R^2	K_p [g/(mg min)]	q_e (mg/g)	q_{e-s} (mg/g)	$t_{1/2}$ (min)	R^2	b	Q_m (mg/g)	Q_{m-s} (mg/g)
Mag	1	0.60	9.86	10.63	0.17	0.998	0.262	20.16	21.72
MicroMag	0.997	0.08	4.95	5.27	2.38	0.987	0.053	13.72	14.60
MagDt-H	0.998	0.33	2.02	11.35	1.48	0.799	0.015	12.31	69.16

calculated by the obtained Fe_3O_4 content (Table 1) and the values of q_e (Table 2) derived from the adsorption kinetic simulation. The values of q_{e-s} for Mag, MicroMag and MagDt-H were obtained as 10.6, 5.3 and 11.4 mg/g, respectively. This result reflects that both diatomite-supported and unsupported magnetite nanoparticles have much higher efficiency on the adsorption and reduction of Cr(VI) than the micron-scaled magnetite particles. Also, the diatomite support has good effect for improving the Cr(VI) removal efficiency of magnetite nanoparticles, which is in accordance with the fact that supported magnetite got better dispersion than their unsupported counterpart.

Fig. 5d displays the Cr(VI) adsorption isotherms of Mag, MicroMag and MagDt-H. The Langmuir equation was used to quantitatively descript the Cr(VI) uptake. The linear form of the Langmuir plot is given as

$$\frac{C_e}{Q_e} = \frac{1}{bQ_m} + \left(\frac{1}{Q_m}\right) C_e \quad (2)$$

where b and Q_m (mg/g) are the Langmuir constant and the monolayer adsorption capacity, respectively, and C_e (mg/L) is the equilibrium concentration of the Cr(VI) in liquid phase. As indicated by the adsorption coefficients computed from Eq. (2) (Table 2), the adsorption isotherms of Mag, MicroMag and MagDt-H well fit the Langmuir model. The monolayer adsorption capacity per unit mass (g) of magnetite content, Q_{m-s}, was calculated by the Fe_3O_4 content (Table 1) and the values of Q_m (Table 2) derived from the Langmuir equation. The Q_{m-s} values of different adsorbents follow an order of MagDt-H (69.2 mg/g) > Mag (21.7 mg/g) > MicroMag (14.6 mg/g). It is noteworthy that the Q_{m-s} value of MagDt-H is also contributed from the adsorption of diatomite support, however, Cr(VI) adsorption of diatomite is very minor relative to that of magnetite so that is overlooked here. This comparison between Q_{m-s} values of various adsorbents indicates that the supporting of diatomite dramatically increases the adsorption capacity of magnetite nanoparticles, providing an additional evidence for the proposal that better dispersion of magnetite nanoparticles results in higher adsorption efficiency.

Further advantages of the heterogeneous diatomite-supported magnetite can be postulated, for example, this material may be much more readily to be pelletized than the unsupported magnetite nanoparticles, and thus be advantageous in actual industrial processes. Moreover, the common uses of diatomite as filter aid and catalytic supports are of help for extending the related applications of supported magnetite.

3.3. Adsorption mechanisms and regeneration tests

The XPS spectra of chromium and iron from the adsorbent surface after adsorption (pH 2.5; initial Cr(VI) concentration 50 mg/L; 120 min) were shown in Fig. 6. The Cr-loaded adsorbents were highlighted in the sample names by adding a suffix "-Cr", i.e., Mag-Cr and MagDt-H-Cr. The Cr2p XPS spectra of Mag-Cr and MagDt-H-Cr exhibit two peaks centered at 577.8 and 586.8 eV (Fig. 6a), assigned to $Cr2p_{3/2}$ and $Cr2p_{1/2}$, respectively [44]. These peaks are typically ascribed to Cr(III), indicating that the Cr(VI) in solution had been adsorbed onto the surface of the adsorbents and then reduced to Cr(III) by a heterogeneous redox process [58,59]. Meanwhile, the Fe2p XPS spectra of Mag-Cr and MagDt-H-Cr showed only fully oxidized iron on the surface, characteristic of the $2p_{3/2}$ peaks centered at ca. 711.8 and 710.5 eV (Fig. 6b), respectively [60]. However, in the Fe2p XPS spectrum of Mag (Fig. 6b), the $2p_{3/2}$ peak is centered at ca. 710.2 eV and the $2p_{1/2}$ peak is at ca. 723.8 eV, which matches well with the data of referenced magnetite [44,60]. Moreover, the values of the binding energy of Fe($2p_{3/2}$) and Fe($2p_{1/2}$) in Mag-Cr and MagDt-H-Cr were higher than that in Mag (Fig. 6b). The increase of the binding energy of Fe($2p_{1/2}$) was previously suggested as an indication of the substitution of Cr(III) for Fe(III) in Cr-substituted magnetites [60,61], so possibly the isomorphic substitution of Fe(III) by Cr(III) took place in Mag-Cr and MagDt-H-Cr, considering that the two ions have similar ionic radii (0.067 nm for

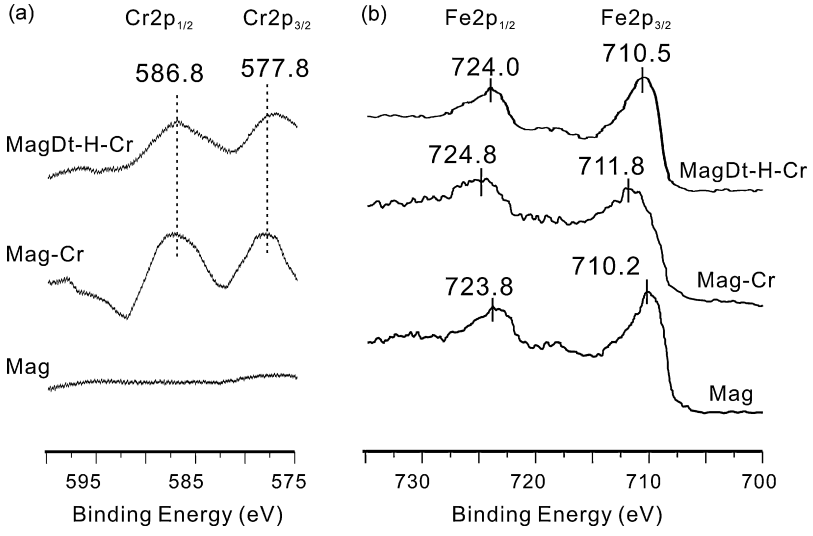

Fig. 6. (a) Cr2p and (b) Fe2p XPS spectra of the synthesized magnetite and Cr-loaded samples.

Fe(III) and 0.065 nm for Cr(III)) and the substitution of Cr(III) for Fe(III) is thermodynamically favored [60]. However, further experimental evidences are still needed for confirming the occurrence of the isomorphic substitution.

The XRD pattern of Mag-Cr (Fig. 1f) should be assigned to the pattern of maghemite rather than magnetite, although both of the two phases have spinel-type structure and exhibit very similar XRD patterns. This assignment is supported by the XPS result that Mag-Cr shows a fully oxidized state, and the relevant DSC curve of Mag-Cr (not shown) also supports the attribution since the exothermic signals of phase-transformation from magnetite to maghemite did not appear any more. Likewise the iron oxide phase in MagDt-H-Cr should be maghemite. Furthermore, a small amount of akaganeite was also found to exist in both Mag-Cr and MagDt-H-Cr as indicated by the XRD patterns (Fig. 1f and g). It should be resulted from the reaction between magnetite and the chlorin-contained solution [44,62]. Moreover, there are no new Cr-contained phases (e.g. chromite, $FeCr_2O_4$) as previously reported [6], found in either Mag-Cr or MagDt-H-Cr. These above results indicate that the magnetite was oxidized into maghemite during the adsorption of Cr(VI), and the resulting Cr(III) species may exist in the surface of the final maghemite-like solid.

A simple regeneration test was conducted to evaluate the reusability of supported/unsupported magnetite nanoparticles. The testing process followed a typical route proposed by Hu et al. [51]: 0.3 g Cr-adsorbed magnetite sample (Mag-Cr or MagDt-H-Cr) was mixed with 5 mL of 0.01 M NaOH solutions for 24 h to remove the adsorbed Cr species, then the obtained magnetite was reused for the Cr(VI) adsorption test, and the above elution/adsorption underwent three cycles. The restored Cr(VI) adsorption capacity (milligram of Cr per gram of actual Fe_3O_4 content) of Mag-Cr was found to be 35.6%, 14.3%, and 6.3% of the original adsorption capacity of Mag, corresponding to the three cycles, respectively, and the values with same meaning for MagDt-H-Cr were 38.7%, 16.9%, and 7.1%, respectively. These results showed that the regeneration of both diatomite-supported/unsupported magnetite nanoparticles was much less inefficient than that of the maghemite nanoparticles [51], whose Cr adsorption capacity remained almost constant even after six cycles of elution/adsorption. This is due to that Cr(VI) adsorption onto maghemite was a reversibly physical process [51], on the contrary, the irreversible redox and isomorphic substitution occurred in the process of Cr(VI) adsorption on magnetite nanoparticles, as revealed by the XPS and XRD results. It is noteworthy that the Cr(VI) adsorption capacity of both Mag-Cr and MagDt-H-Cr was partially restored after 1 cycle of elution/adsorption, suggesting some Cr species adsorbed by electrostatic attraction were released and thus the corresponding adsorption sites were freed for next adsorption. However, after 3 cycles of elution/adsorption most of the Cr species were finally fixed into the adsorbents through redox and isomorphic substitution. According to the discussion based on the XPS and XRD results, it can be postulated that the final product after regeneration would be a Cr-loaded iron oxide solid with maghemite-like structure. As reported in literatures [60,61], these sort of Cr-containing iron oxides is of high prospect for the catalytic uses. Accordingly, the regeneration of the diatomite-supported/unsupported magnetite nanoparticles may be of meaning in not only recovering the adsorbent itself but also making use of the useful Cr components. Testing on this potential use will be done as part of another investigation.

4. Conclusions

Diatomite-supported magnetite nanoparticles can be prepared by both co-precipitation and hydrosol method. The supported magnetite nanoparticles synthesized via hydrosol method are better dispersed and less coaggregated than those synthesized via co-precipitation method and the unsupported magnetite nanoparticles.

The Cr(VI) uptake onto these synthesized magnetite nanoparticles was a physico-chemical process, including an electrostatic attraction followed by a redox process in which Cr(VI) was reduced into Cr(III). For a given sample, the adsorption of Cr(VI) was strongly affected by the pH values and the kinetics of the adsorption followed the pseudo-second-order model. The Cr(VI) adsorption data of unsupported/supported magnetite fit well with the Langmuir isotherm equation.

The diatomite-supported magnetite synthesized via hydrosol method exhibited a higher adsorption capacity per unit mass of magnetite (q_{e-s}, 11.4 mg/g), calculated from the pseudo-second-order kinetics equation, than the unsupported nano-scaled magnetite (10.6 mg/g) and the micron-scaled magnetite (5.3 mg/g). The monolayer adsorption capacities per unit mass (g) of magnetite content (Q_{m-s}) of these materials, obtained from the simulation with the Langmuir equation, followed a similar order of diatomite-supported nano-scaled magnetite (69.2 mg/g) > unsupported nano-scaled magnetite (21.7 mg/g) > micron-scaled magnetite (14.6 mg/g). These results indicate that diatomite support is useful on improving the Cr(VI) adsorption capacity. Furthermore, supporting of diatomite is of help for the storage and pelletization of the magnetite nanoparticles. These fundamental results demonstrate that the diatomite-supported/unsupported magnetite nanoparticles are readily prepared, enabling promising applications for the removal of Cr(VI) from aqueous solution.

Acknowledgements

This is a contribution (No. IS-1111) from GIGCAS. Financial supports from the National Natural Scientific Foundation of China (Grant No. 40872042) and the Knowledge Innovation Program of the Chinese Academy of Sciences (Grant No. GIGCX-07-11/21) are gratefully acknowledged. The authors thank Dr. Jingming Wei for her assistance in the characterization work by using N_2 adsorption–desorption isotherms.

References

[1] I.M. Hsing, Y. Xu, W.T. Zhao, Micro- and nano-magnetic particles for applications in biosensing, Electroanalysis 19 (2007) 755–768.
[2] A.F. Ngomsik, A. Bee, M. Draye, G. Cote, V. Cabuil, Magnetic nano- and microparticles for metal removal and environmental applications: a review, Comptes Rendus Chimie 8 (2005) 963–970.
[3] N.A. Booker, D. Keir, A.J. Priestley, C.B. Ritchie, D.L. Sudarmana, M.A. Woods, Sewage clarification with magnetite particles, Water Sci. Technol. 23 (1991) 1703–1712.
[4] J.D. Orbell, L. Godhino, S.W. Bigger, T.M. Nguyen, L.N. Ngeh, Oil spill remediation using magnetic particles—an experiment in environmental technology, J. Chem. Educ. 74 (1997) 1446–1448.
[5] L.C.A. Oliveira, R.V.R.A. Rios, J.D. Fabris, K. Sapag, V.K. Garg, R.M. Lago, Clay-iron oxide magnetic composites for the adsorption of contaminants in water, Appl. Clay Sci. 22 (2003) 169–177.
[6] J. Hu, I.M.C. Lo, G. Chen, Removal of Cr(VI) by magnetite nanoparticle, Water Sci. Technol. 50 (2004) 139–146.
[7] S.S. Banerjee, D.H. Chen, Fast removal of copper ions by gum arabic modified magnetic nano-adsorbent, J. Hazard. Mater. 147 (2007) 792–799.
[8] N. Feltin, M.P. Pileni, New technique to make ferrite nanosized particles, J. Phys. IV 7 (1997) 609–610.
[9] R.F. Ziolo, E.P. Giannelis, B.A. Weinstein, M.P. Ohoro, B.N. Ganguly, V. Mehrotra, M.W. Russell, D.R. Huffman, Matrix-mediated synthesis of nanocrystalline gamma-Fe_2O_3—a new optically transparent magnetic material, Science 257 (1992) 219–223.
[10] M.J. Zhang, Q. Zhang, T. Itoh, M. Abe, Ferrite plating on porous silica microspheres for ultrasonic contrast agents, IEEE Trans. Magn. 30 (1994) 4692–4694.
[11] A.A. Novakova, V.Y. Lanchinskaya, A.V. Volkov, T.S. Gendler, T.Y. Kiseleva, M.A. Moskvina, S.B. Zezin, Magnetic properties of polymer nanocomposites containing iron oxide nanoparticles, J. Magn. Magn. Mater. 258 (2003) 354–357.

[12] Y.S. Kang, S. Risbud, J. Rabolt, P. Stroeve, Brewster angle microscopy study of a magnetic nanoparticle/polymer complex at the air/water interface, Langmuir 12 (1996) 4345–4349.
[13] I.J. Bruce, J. Taylor, M. Todd, M.J. Davies, E. Borioni, C. Sangregorio, T. Sen, Synthesis, characterisation and application of silica–magnetite nanocomposites, J. Magn. Magn. Mater. 284 (2004) 145–160.
[14] C. Galindo-Gonzalez, J. de Vicente, M.M. Ramos-Tejada, M.T. Lopez-Lopez, F. Gonzalez-Caballero, J.D.G. Duran, Preparation and sedimentation behavior in magnetic fields of magnetite-covered clay particles, Langmuir 21 (2005) 4410–4419.
[15] M. Arruebo, R. Fernandez-Pacheco, S. Irusta, J. Arbiol, M.R. Ibarra, J. Santamaria, Sustained release of doxorubicin from zeolite–magnetite nanocomposites prepared by mechanical activation, Nanotechnology 17 (2006) 4057–4064.
[16] A. Murathan, S. Benli, Removal of Cu^{2+}, Pb^{2+} and Zn^{2+} from aqueous solutions on diatomite via adsorption in fixed bed, Fresen. Environ. Bull. 14 (2005) 468–472.
[17] Z.H. Zhang, Z.Y. Wang, Diatomite-supported Pd nanoparticles: an efficient catalyst for Heck and Suzuki reactions, J. Org. Chem. 71 (2006) 7485–7487.
[18] M. Gabrovska, J. Krstic, R. Edreva-Kardjieva, M. Stankovic, D. Jovanovic, The influence of the support on the properties of nickel catalysts for edible oil hydrogenation, Appl. Catal. A: Gen. 299 (2006) 73–83.
[19] P. Yuan, D.Q. Wu, H.P. He, Z.Y. Lin, The hydroxyl species and acid sites on diatomite surface: a combined IR and Raman study, Appl. Surf. Sci. 227 (2004) 30–39.
[20] L. Dupont, E. Guillon, Removal of hexavalent chromium with a lignocellulosic substrate extracted from wheat bran, Environ. Sci. Technol. 37 (2003) 4235–4241.
[21] U. Förstner, G.T.W. Wittmann, Metal Pollution in the Aquatic Environment, 2nd rev. ed., Springer-Verlag, Berlin/New York, 1981.
[22] J.G. Dean, F.L. Bosqui, K.H. Lanouette, Romoving heavy metals from waste water, Environ. Sci. Technol. 6 (1972) 518–522.
[23] V.K. Gupta, C.K. Jain, I. Ali, M. Sharma, V.K. Saini, Removal of cadmium and nickel from wastewater using bagasse fly ash—a sugar industry waste, Water Res. 37 (2003) 4038–4044.
[24] S. Rengaraj, C.K. Joo, Y. Kim, J. Yi, Kinetics of removal of chromium from water and electronic process wastewater by ion exchange resins: 1200H, 1500H and IRN97H, J. Hazard. Mater. 102 (2003) 257–275.
[25] R. Aravindhan, B. Madhan, J.R. Rao, B.U. Nair, T. Ramasami, Bioaccumulation of chromium from tannery wastewater: an approach for chrome recovery and reuse, Environ. Sci. Technol. 38 (2004) 300–306.
[26] R.R. Patterson, S. Fendorf, M. Fendorf, Reduction of hexavalent chromium by amorphous iron sulfide, Environ. Sci. Technol. 31 (1997) 2039–2044.
[27] M. Pettine, L. D'Ottone, L. Campanella, F.J. Millero, R. Passino, The reduction of chromium (VI) by iron (II) in aqueous solutions, Geochim. Cosmochim. Acta 62 (1998) 1509–1519.
[28] M. Erdem, F. Tumen, Chromium removal from aqueous solution by ferrite process, J. Hazard. Mater. 109 (2004) 71–77.
[29] M.J. Alowitz, M.M. Scherer, Kinetics of nitrate, nitrite, and Cr(VI) reduction by iron metal, Environ. Sci. Technol. 36 (2002) 299–306.
[30] T. Astrup, S.L.S. Stipp, T.H. Christensen, Immobilization of chromate from coal fly ash leachate using an attenuating barrier containing zero-valent iron, Environ. Sci. Technol. 34 (2000) 4163–4168.
[31] J.P. Gould, The kinetics of hexavalent chromium reduction by metallic iron, Water Resour. 16 (1982) 871–877.
[32] T. Lee, H. Lim, Y. Lee, J.W. Park, Use of waste iron metal for removal of Cr(VI) from water, Chemosphere 53 (2003) 479–485.
[33] S.M. Ponder, J.G. Darab, T.E. Mallouk, Remediation of Cr(VI) and Pb(II) aqueous solutions using supported, nanoscale zero-valent iron, Environ. Sci. Technol. 34 (2000) 2564–2569.
[34] R.M. Powell, R.W. Puls, S.K. Hightower, D.A. Clark, Corrosive and geochemical mechanisms influencing in situ chromate reduction by metallic iron, in: 209th ACS National Meeting, American Chemical Society, Anaheim, California, 1995.
[35] A.G.B. Williams, M.M. Scherer, Kinetics of Cr(VI) reduction by carbonate green rust, Environ. Sci. Technol. 35 (2001) 3488–3494.
[36] M. Erdem, F. Gur, F. Tumen, Cr(VI) reduction in aqueous solutions by siderite, J. Hazard. Mater. 113 (2004) 219–224.
[37] A.F. White, M.L. Peterson, Reduction of aqueous transition metal species on the surfaces of Fe(II)-containing oxides, Geochim. Cosmochim. Acta 60 (1996) 3799–3814.
[38] M.L. Peterson, G.E. Brown, G.A. Parks, C.L. Stein, Differential redox and sorption of Cr(III/VI) on natural silicate and oxide minerals: EXAFS and XANES results, Geochim. Cosmochim. Acta 61 (1997) 3399–3412.
[39] P. Yuan, D. Yang, Z. Lin, H. He, X. Wen, L. Wang, F. Deng, Influences of pretreatment temperature on the surface silylation of diatomaceous amorphous silica with trimethylchlorosilane, J. Non-cryst. Solids 352 (2006) 3762–3771.
[40] Y.S. Kang, S. Risbud, J.F. Rabolt, P. Stroeve, Synthesis and characterization of nanometer-size Fe_3O_4 and gamma-Fe_2O_3 particles, Chem. Mater. 8 (1996) 2209–2211.
[41] M.S. Rand, A.E. Greenberg, M.J. Taras, Standard Methods for the Examination of Water and Wastewater, 16th ed., American Public Health Association, New York, 1975.
[42] S.J. Gregg, K.S.W. Sing, Adsorption, Surface Area and Porosity, 2nd ed., Academic Press, London, 1982.
[43] E.P. Barrett, L.G. Joyner, P.P. Halenda, Determination of pore volume and area distribution in porous substances, J. Am. Chem. Soc. 73 (1951) 373–380.
[44] R.M. Cornell, U. Schwertmann, The Iron Oxides: Structure, Properties, Reactions, Occurrences and Uses, Wiley-VCH, Weinheim, 2003.
[45] J. Mazo-zuluaga, C.A. Barrero, J. Diaz-Teran, A. Jerez, Thermally induced magnetite–haematite transformation, Hyperfine Interact. 148/149 (2003) 153–161.
[46] Q. He, S. Guo, W. Wu, R. Hu, J. Huang, Monodisperse magnetite nanoparticles synthesis and their thermal-stability, in: The 1st International Conference on Bioinformatics and Biomedical Engineering (ICBBE 2007), Wuhan, China, 2007.
[47] P. Yuan, H.P. He, F. Bergaya, D.Q. Wu, Q. Zhou, J.X. Zhu, Synthesis and characterization of delaminated iron-pillared clay with meso-microporous structure, Micropor. Mesopor. Mater. 88 (2006) 8–15.
[48] P. Yuan, X.L. Yin, H.P. He, D. Yang, L.J. Wang, J.X. Zhu, Investigation, on the delaminated-pillared structure of TiO_2-PILC synthesized by TiC1(4) hydrolysis method, Micropor. Mesopor. Mater. 93 (2006) 240–247.
[49] M.W. Anderson, S.M. Holmes, N. Hanif, C.S. Cundy, Hierarchical pore structures through diatom zeolitization, Angew. Chem. Int. Ed. 39 (2000) 2707–2710.
[50] M. Perezcandela, J.M. Martinmartinez, R. Torregrosamacia, Chromium(VI) removal with activated carbons, Water Res. 29 (1995) 2174–2180.
[51] J. Hu, G.H. Chen, I.M.C. Lo, Removal and recovery of Cr(VI) from wastewater by maghemite nanoparticles, Water Res. 39 (2005) 4528–4536.
[52] P.A. Brown, S.A. Gill, S.J. Allen, Metal removal from wastewater using peat, Water Res. 34 (2000) 3907–3916.
[53] S. Babel, E.M. Opiso, Removal of Cr from synthetic wastewater by sorption into volcanic ash soil, Int. J. Environ. Sci. Technol. 4 (2007) 99–107.
[54] S.B. Lalvani, A. Hubner, T.S. Wiltowski, Chromium adsorption by lignin, Energ. Source 22 (2000) 45–56.
[55] E. Demirbas, M. Kobya, E. Senturk, T. Ozkan, Adsorption kinetics for the removal of chromium (VI) from aqueous solutions on the activated carbons prepared from agricultural wastes, Water SA 30 (2004) 533–539.
[56] Y.S. Ho, G. McKay, Pseudo-second order model for sorption processes, Process. Biochem. 34 (1999) 451–465.
[57] Y.S. Ho, J.C.Y. Ng, G. Mckay, Removal of lead(II) from effluents by sorption on peat using second-order kinetics, Sep. Sci. Technol. 36 (2001) 241–261.
[58] M.L. Peterson, G.E. Brown, G.A. Parks, Direct XAFS evidence for heterogeneous redox reaction at the aqueous chromium/magnetite interface, Colloid Surf. A 107 (1996) 77–88.
[59] M.L. Peterson, A.F. White, G.E. Brown, G.A. Parks, Surface passivation of magnetite by reaction with aqueous Cr(VI): XAFS and TEM results, Environ. Sci. Technol. 31 (1997) 1573–1576.
[60] J. Manjanna, G. Venkateswaran, Effect of oxidative pretreatment for the dissolution of Cr-substituted hematites/magnetites, Ind. Eng. Chem. Res. 41 (2002) 3053–3063.
[61] F. Magalhaes, M.C. Pereira, S.E.C. Botrel, J.D. Fabris, W.A. Macedo, R. Mendonca, R.M. Lago, L.C.A. Oliveira, Cr-containing magnetites $Fe_{3-x}Cr_xO_4$: the role of Cr^{3+} and Fe^{2+} on the stability and reactivity towards H_2O_2 reactions, Appl. Catal. A: Gen. 332 (2007) 115–123.
[62] E. Tombácz, E. Illés, A. Majzik, A. Hajdú, N. Rideg, M. Szekeres, Ageing in the inorganic nanoworld: example of magnetite nanoparticles in aqueous medium, Croat. Chem. Acta 80 (2007) 503–515.